Comparative Assessment of Injection Strategies for Highly Concentrated Nano Fe/Cu Particles into Sand Columns

Comparative Assessment of Injection Strategies for Highly Concentrated Nano Fe/Cu Particles into Sand Columns

Published in

Journal of Environmental Engineering

Volume 141, Issue 4, 1 April 2015, Article number 04014077

Tiziana Tosco[1] and Seiyed Mossa Hosseini[2]

[1]Assistant Professor, Dipartimento di Ingegneria dell'Ambiente, del Territorio e delle Infrastrutture, Politecnico di Torino,Torino, Italy. E-mail address: tiziana.tosco@polito.it

[2]Assistant Professor, Natural Geography Department, University of Tehran, Tehran, P.O.Box: 14155-6465, Iran. E-mail address: smhosseini@ut.ac.ir

Abstract

The transport of bimetallic nano-*Fe/Cu* particles through coarse sand-packed columns was investigatedsimulating particle transport under 25 injection strategy scenarios. The considered transport mechanisms included retention on and release from the solid grains, modeled by a dual-site advection-dispersion-deposition equation, and clogging of the porous medium. The transport kinetics and parameters used in this study were calibrated against experimental data, previously reported, and simulated using E-MNM1D. The influence of the injected particle concentration(2 to 12 g/l), flow rate (43.2 to 172.8 m/d), duration,and eventual alternation of injection and flushing periods was analyzed. The impact of each scenario was quantified in terms of particle mobility, porous medium clogging, water pressure, and uniformity of distribution of the particles in the porous medium.The results of this study indicate that, when injecting under conditions typical of a full-scale aquifer remediation, nanoparticle mobility and distribution are optimized and clogging is minimized by using high flow rates, low concentrations, and frequent injection steps without intermediate flushing.

Subject Headings

Colloids, Transport phenomena, Nanotechnology, Porous media, Groundwater, Remediation

Introduction

The injection of nanosized zerovalent iron particles (NZVI) represents one of the most innovative technologies for in-situ remediation of contaminatedaquifer systems, thanks to the high reactivity of suchparticles towards a broad range of contaminants(Fiore and Zanetti 2009; Freyria et al. 2011; Phenrat et al. 2011; Saleh et al. 2008; Tosco et al. 2014; Zanetti and Fiore 2005; Zhang 2003; Zolla et al. 2009). However, the NZVI mobilityin the subsurfaceis very limited when particles are injected without any surface amendment (eg adsorbed polymers, oil-in-water emulsions, particle coating with doping metals, etc.)(Johnson et al. 2009; Phenrat et al. 2010; Tiraferri et al. 2008; Tratnyek and Johnson 2006).Bare NZVI exhibits a strong tendency to aggregate, agglomerate, and consequently to settle rapidly onto the solid phase. This effect is especially marked for high NZVI concentrations (1 to 20 *g/l*), in the typical range required for field applications (Cantrell et al. 1997; Nurmi et al. 2005; Nyer and Vance 2001), and is extremely detrimental for field applications (Noubactep et al. 2012; Tiraferri and Sethi 2009).Excessive particle retention clogs the pores in the vicinityof the injection point, resulting in asignificant loss of porosity and permeability, and in a very limited radius of influence of the injection. Continued injection under pressure will ultimately create preferential pathways, which strongly limit the contact between iron particles and contaminants, thereby reducing the effectiveness of remediation (Huang and Zhang 2005; Tosco and Sethi 2010; Westerhoff and James 2003).In recent years, great efforts have been consequently devoted to identify effective, non-harmful, and economically affordable strategies to improve the colloidal stability of NZVI dispersions(Tosco et al. 2014). The approachesexplored so far include (i) modification of the particle surface properties to increase repulsion via adsorptionof natural orsyntheticpolymers (starch, poly-acrylic acid, carboxymethyl cellulose, guar gum, etc.) (He and Zhao 2005; Kanel et

al. 2008; Phenrat et al. 2007; Schrick et al. 2004; Tiraferri et al. 2008); (ii) partial coatingof the particle surface during synthesis (Sakulchaicharoen et al. 2010) or inclusion in oil emulsions(Quinn et al. 2005); (iii) improvement of the propertiesof the dispersant fluid using shear-thinning polymeric solutions (Comba et al. 2011; Comba and Sethi 2009; Dalla Vecchia et al. 2009; Johnson et al. 2009; Tiraferri et al. 2008; Xue and Sethi 2012), which reduce aggregation and sedimentation by increasing itsviscosity.

Beside colloidal stability, anumber offactors have also been identified that may significantly affect the mobility of NZVI in the subsurface, as summarized in Figure 1. These factors includethe geochemical properties of the subsurface water and/or dispersing water (namelypH, ionic strength and dissolved species) (Bunn et al. 2002; Ryan et al. 2000; Saleh et al. 2008; Tiraferri et al. 2011; Tosco et al. 2009), physical characteristics of the aquifer (namely grain size, porosity and permeability)(Kim et al. 2007), spatial heterogeneitiesin theaquifer properties and contaminant concentration in the plume (Phenrat et al. 2011), depth of the contaminated area(Cook 2009), and specificcharacteristics of the NZVI, such as magnetic attractive forces (related to Fe^0 content) and size distribution(Phenrat et al. 2009). Finally, also the injection strategy, i.e. the operating conditions during NZVI injection, is known to control the mobility and the final fate of the injected particles. In particular, the injection rate (and thus the pore water velocity in dynamic conditions)(Bai and Tien 1999; Hosseini et al. 2011)and the delivered NZVI concentration are relevant parameters(Hosseini and Tosco 2013; Phenrat et al. 2010; Phenrat et al. 2009; Saleh et al. 2008).

The wide variety of factors reported in Figure 1and the complexity of the possible interactions among them make a comprehensive study unfeasible (Chen et al. 2001). It should be also mentioned that, among the four sets of factors reported in Figure 1, only the characteristics of

particles and dispersant fluid as well as the injection strategy are fully in our control. Numerousresearchers investigated the effects of one or more factors on the transport and retention of NZVI in well-controlled lab-scale columns (Nyer and Vance 2001; Phenrat et al. 2010; Saleh et al. 2008; Tiraferri and Sethi 2009), including particle stabilization methods, groundwater ionic strength and ion valence(Phenrat et al. 2010; Saleh et al. 2008; Tosco et al. 2012),particle size and composition, flow rate, and heterogeneities in the porous material (Hosseini and Tosco 2013; Kim et al. 2012; Phenrat et al. 2010). Conversely, few studies have been devoted to understand the roleof the injection strategy, and to our knowledge no systematic study has beenreported to date concerning the impact of different injection strategies (flow rate, NZVI concentration, injection duration and alternation with flushing) on NZVI mobility. When injecting NZVI slurries into the subsoil, the optimal injection strategy should provide a reasonable radius of influence (whose extent should be tunable by the operator) with the minimum impact of NZVI deposits on the porous medium permeability, to avoid the bypass of the reactive zone when natural flow conditions are restored. Phenrat *et al*. (2011) showed that, in the presence of a NAPL phase, NZVIcantarget theNAPL/water interface more efficiently when injected at lower flow rates and for a longer time, compared to fast single-stepNZVI delivery.

In this study, a quantitative analysis is conductedon how the management of the injection of NZVI water-based slurriescan optimize themobility of the particles.In particular, the impact of injected NZVI concentration, flow rate, and number, duration, and alternation ofinjection and flushing periods is considered. NZVI transport simulations in 1D domains were performed using E-MNM1D (Tosco and Sethi 2010) for bimetallic nano-*Fe/Cu* particles, whose transport was previously assessed by the authors in laboratory column tests (Hosseini and Tosco 2013). Several injection scenarios were considered, including single-step injections (injection followed by

flushing), and multi-steps injections (repetition of injection+flushing steps) with constant and variable particle concentration. The performance of each scenario was quantifiedin terms of travel distance, changes in porous medium porosity, permeability, and overpressure during injection.

Material and Methods

The mobility and retention of highly concentrated dispersions of bimetallic *Fe/Cu* nanoparticles (d_{50} = 70 ± 5 *nm*, BET surface area *SA*= 28.6 $m^2\ g^{-1}$, and particle density ρ_p = 7550 $kg\ m^{-3}$) throughcolumns(0.5 *m* length and 0.025 *m* inner diameter) packed with coarse sand (d_{50}= $0.83\times10^{-3}m$) was investigated in a previous work(Hosseini and Tosco 2013). In particular, the influence of high flow rate (*V* = 43.2, 86.4, and 172.8 *m/d*) and injected particle concentrations (C_{inj}= 2, 5, 8 and 12 $g\ l^{-1}$) was addressed. The ionic strength of flushing water (40 *mM*, constant during the experiments) mimicked the fresh groundwater used for the water supply of the city of Karaj (Iran). The experimental data (breakthrough curves and pressure drop logs over time) were modeledusing the software E-MNM1D(Tosco et al. 2014; Tosco and Sethi 2010), which provides a numerical solution to colloid transport equations (advection-dispersion-deposition processes) coupled to clogging. E-MNM1D is available for free download at www.polito.it/groundwater/software both as a Matlab-based code with Excel interface, and as a part of the colloid transport simulation software MNMs 2014 (with a graphical interface).

Colloid transport equations and numerical solution

E-MNM1D (Tosco and Sethi 2010)solves the 1-Dcolloid transport equation in saturated porous media with two concurrent kinetics of particle deposition and resuspension to and from the soil

matrix. The set of partial differential equations describing the coupled flow and transportof colloidal suspensions with associated clogging can be written as follows:

$$\frac{\partial}{\partial t}(\varepsilon C)+\frac{\partial}{\partial t}(\rho_b s)=\frac{\partial}{\partial x}(q C)+\frac{\partial}{\partial x}\left(\varepsilon D_x \frac{\partial C}{\partial x}\right) \tag{1}$$

$$\frac{\partial}{\partial t}(\rho_b s_1)=\varepsilon k_{a1}\left(1+A_1 s_1^{\beta_1}\right)C-\rho_b k_{d1} s_1 \tag{2}$$

$$\frac{\partial}{\partial t}(\rho_b s_2)=\varepsilon k_{a2}\left(1+\frac{x}{d_{50}}\right)^{\beta_2} C-\rho_b k_{d2} s_2 \tag{3}$$

$$\varepsilon(s)=n-\frac{\rho_b}{\lambda\rho_p}s \tag{4}$$

$$a(s)=a_0+\theta a_p \frac{\rho_b}{\rho_p}s \tag{5}$$

$$K(s)=K_0\left[\frac{\varepsilon}{n}\right]^3\left[\frac{a_0}{a}\right]^2 \tag{6}$$

$$-\nabla p=\frac{\mu}{K(s)}q \tag{7}$$

where x [L] and t [T] are the independent variables for space and time, respectively; C [ML^{-3}] and s [M/M]are the concentration of particles suspended in the fluid phase and deposited on the soil matrix, D_x[L^2T^{-1}] is the hydrodynamic dispersion, q [LT^{-1}] the Darcyan flow velocity, ρ_b [ML^{-3}]the porous medium bulk density,ε [-] the effective porosity, k_a^i and k_d^i [T^{-1}]the deposition and release rate coefficients for the i^{th} interaction site (i=1, 2),A_i and β_i [-] the multiplier and exponent coefficients defining the interaction dynamics,d_{50} [L] the mean diameter of the porous material, n [-] the initial porosity of the porous medium before the injection of the particles, a_0 [L^{-1}] the

specific surface area of the porous matrix, a_p [L^{-1}] the specific surface area of the nanoparticles, ρ_p [ML^{-3}] the density of the nanoparticles,λ [-]the average degree of packing of the particle deposits,θ the fraction of deposited nanoparticles contributing to the overall increase of the interface area [-], $K(s)$ the permeability coefficient expressed as a function of the concentration of deposited particles [L^2], K_0 the permeability coefficient in the absence of deposited particles,μ the dynamic viscosity of the pore fluid [$ML^{-1}T^{-1}$], q the darcyan flow velocity [$L\ T^{-1}$], and ∇p the pore pressure gradient [$ML^{-1}T^{-2}$].

Two reversible particles deposition/release sites were considered ($s = s_1 + s_2$): site 1 is a generic formulation which can be adapted to all commonly used interaction kinetics (first-order deposition dynamics if $A_1 = 0$, blocking if $A_1 < 0$, ripening if $A_1 > 0$) and site 2 considers the space-dependent deposition dynamics following straining kinetics(Bradford et al. 2003).The reader can refer to previous works for a detailed discussion on the colloid transport mechanisms and model equations (Tosco et al. 2014; Tosco and Sethi 2009; Tosco and Sethi 2010).

The following initial conditions for $C(x,t)$ and $s(x,t)$ were applied:

$$C(x, t = 0) = 0 \tag{8}$$

$$s_i(x, t = 0) = 0 \qquad i = 1, 2 \tag{9}$$

A zero-gradient boundary condition was applied at the column outlet ($x = L$). To define the boundary condition at the column entrance (x=0), different particle-injection strategieswere employed. Each strategy includes alternated stress periods of particle injection (with particle concentration C_{inj} constant during the stress period) and flushing (without particle injection). The model providesresults in terms of particle transport (breakthrough curves and profiles of

deposited iron concentration), water pressure drop over time, changes in theeffective porosity,and permeability over space and time.

Transients in the flow field were assumed negligible, and consequently the problem was solved as a quasi-stationary phenomenon, and Darcy's law was applied to calculatethe pressure gradient. In the numerical solution of the set of model equations, the flow rate was updated for each stress period and assumed equal to the imposed inlet flow rate, while permeability was calculated at each time step.

Injection strategies of nano-Fe/Cu particles

In a previous work (Hosseini and Tosco 2013), the inverse modeling of experimental results with the equations (1-9) provided three sets of transport parameters, one for each flow rate, which were found independent of the injected concentration. In this study, such values of the transport parameters were used in the transport simulations (Table 1). The three flow rate values were selected as representative, respectively, of near-well conditions, intermediate distance, and longer distance from the injection well (Table 2), following Johnson *et al*. (2009). Please note that the parameter A_1 is positive for all applied flow rates, suggesting that the deposition of particles onto the porous medium follows a ripening dynamics.

Twenty five different injection strategies were defined (Table **2**, 3and4). Foreach strategy,a transport simulation was run using E-MNM1D in direct (predictive) mode, and the results were analyzed in terms of eluted and retained NZVI concentration, variation in pressure drop, effective porosity, and porous medium permeability over time. For each strategy, three simulations were run imposing three pore water velocities (43.2, 86.4, and 172.8 m/d) for a total number of 75 (25×3) simulations. The flow rate was kept constant during each simulation.

To make the results of different injection strategiescomparable among each other, the overall duration of the simulated experiment, t_{exp} (i.e. duration of injection + flushing steps),and the total injected mass of NZVI, *TIM*, were the same in all simulations (see also Tables 3 and 4):

$$t_{exp} = \sum_{i=1}^{n} t_{inj}^{i} + \sum_{j=1}^{m} t_{flush}^{j} = 40000\ s \quad (10)$$

$$TIM = \sum_{i=1}^{n} F_{inj}^{i} \times t_{inj}^{i} = 32600\ kg/m^3 \quad (11)$$

where*n* and *m* are respectively, the number of injection and flushing periods in each strategy. It should be mentioned that the value of t_{exp}=4000 s is valid only for pore water velocity of 43.2 m/d, whereas for the cases of 86.4 and 172.8 m/d (t_{inj}) must be reduced to imposethe same injection fluxes.

The experimental results reported in the previous study (Hosseini and Tosco 2013) evidenced that, for high NZVI concentrations (particularly 8 and 12 gl^{-1}), the pressure drop at column ends, which is directly related to clogging phenomena, is expected to significantly increase after ~600 seconds. Therefore, pore plugging can be minimized if NZVI injection is stopped before the pressure begins to grow. For this reason, injection times lower than 600 seconds were considered in the strategies herein investigated. However, for two strategies (strategies #S2 and #S3 as define following) a prolongedinjection time wasadoptedfor comparison.

More in details, the injection strategies can be classified into four setsbased on several prior trails:

1. First set: strategies #S1 to #S3 (Table 3):experiments include two stress periods (Figure 2a), namely one injection followed by one flushing step, characterized bydifferent duration, NZVI mass flux F_{inj}, and injected particle concentration C_{inj}.

2. Second set: strategies #S4 to #S11 (Table 3): the effects of oneflushing step between two injections and of different injected concentrations are investigated (Figure 2b-d). The overall duration of the injection is the same for all tests, while the duration of flushing periods varies.
3. Third set:Strategies #S12 to#S22 (Table 3):experiments include three injection steps, each followed by a flushing step. (Figure 2e-h). Also in these cases, the overall duration of the three injection stress periods is the same for all tests, regardless the injected concentration, while the injected concentration and the duration of flushing stepsvaries.
4. Fourth set: Strategies #S23 to #S25 (Table 4): the effects of a gradual variation of injected concentration is investigated, simulating the continuous injection of particles divided intonine injection steps characterized by a gradual variation in the NZVI concentration (Figure 3).

Evaluation Criteria

For comparisonamongthe simulation results ofthe 25 strategies, the following evaluation criteria were calculated:

- Criterion $C1_{\Delta P}$: Percentage of increase in maximum pressure drop: for a given strategy;this criterioncompares the peak in pressure drop at column ends(due to clogging)with the initial (clean bed) pressure drop (ΔP_0):

$$C1_{\Delta P} = \frac{\Delta P_{max} - \Delta P_0}{\Delta P_0} \times 100 \quad (12)$$

where ΔP_{max} is the maximum pressure drop reached during the simulation.

The pressure drop along the column is directly related to the pore water velocity through the Darcy's law. In clean bed conditions (i.e. no particles retained),a pressure drop equal to ΔP_0 = 1114.08, 2228.16, and 4456.34 *Pa* was calculated, forthe three considered flow velocities *V*=43.2, 86.4, and 172.8m/d, respectively.

- Criterion $C2_{C/Cinj}$: Percentage of retained mass: the percentage of total mass of NZVIretained within the 0.5 m long domainat the end of the simulation is considered. The integral of the normalized breakthrough curve C/C_{inj} was used to calculate the mass balance:

$$C2_{C/C_{inj}} = \left(1 - \frac{\int_0^{t_{\exp}} {}^{C}/_{C_0} dt}{\sum_{j=1}^{n} t_{inj}^{j}}\right) \times 100 \qquad (13)$$

where*n* is number of injection periods for the given strategy.

- Criterion $C3_{AEP}$: Percentage of reduction in averaged effective porosity. The effective porosity averaged along the column (*AEP*), directly related to the pressure drop,was calculated as the integral of the space-dependent porosity:

$$AEP(t) = \frac{1}{L}\int_0^L \varepsilon(x,t)dx \qquad \text{for } t\text{= 0to } t_{exp} \qquad (14)$$

where*L* is the column length. In the $C3_{AEP}$criterion, the maximum loss in AEP was calculated as the ratio of the minimum *AEP* (AEP_{min}) to the initial *AEP* (AEP_0= *n=0.37*):

$$C3_{AEP} = \frac{AEP_0 - AEP_{min}}{AEP_0} \times 100 \qquad (15)$$

- Criterion $C4_K$: Percentage of reduction in permeability, which is related to the normalized effective porosity and normalized specific surface area of the porous medium through the Kozeny-Carman equation (eq. 6). The average permeability along the column at the end of the experiment(K_a) was calculated by applying an integral in space(similarly to eq. 14) and comparing the resultto the initial (clean bed)permeability (K_0=5.6 × $10^{-11} m^2$):

$$C4_K = \frac{K_0 - K_a}{K_0} \times 100 \quad (16)$$

All the criteria refer to different critical effects of NZVI injection, and can be directly applied to compare the different strategies: the lower the values, the better the performance of the injection strategy in terms of improving mobility of the injected NZVI and minimizing clogging. As a further criterion, the distance over which 99% of the particles are retained ($L_{99\%}$) was calculated ($C5_{L99\%}$). To this aim, the model domain was extended up to several meters in order to get a zero breakthrough at the exit in all conditions, and the travel distance was calculated from the simulated profiles of retained particle concentration.For a better comparison of the efficacy of the considered strategies based on the criterion$C5_{L99\%}$, the injection strategy which produced the lowest$L_{99\%}$was considered as the benchmark (referred to asl_b) and the travel lengths obtained from all other strategies were evaluated against this benchmark, and expressed as a relative travel distancewith respect to l_b.

Results and Discussion

Criterion $C1_{\Delta P}$: pressure drop

The five criteriawerecalculatedfrom thecorresponding simulated results of EMNM1D for each strategy and flow rate.The values of criterion$C1_{\Delta P}$ (percentage of increase in maximum pressure drop) are summarized in the bar-plot of Figure 4. Consistentlywith Darcy's law, the maximum pore water pressure increases with increasing pore water velocity. This effect is more relevant for strategies S1, S2 and also S6 to S11. The fourth set of strategies S23-S25 (S25 in particular) corresponds tothe minimum increase in pressure drop (i.e. minimum $C1_{\Delta P}$), while the strategy S1 corresponds to the maximum drop. For comparison, Figure 5 reports the profile of water pressure drop versus time of the simulated injections for strategies S1 and S23for V=43.2 and V=172.8 m/d. In S1, a constant NZVI concentration equal to16 *g/l* was injected for 545 *s*, while in S23 an average concentration C_{inj} of 1.8 *g/l*, with peak concentration of 3.3 *g/l*, was injected for an overall duration of 525 *s*× 9 = 4725 *s*. In other words, the injection of lower concentrations with a gradual variation of C_{inj} (in a triangular shape) has the lowest hydrological impactcompared to particles injected athigher and constant concentration. Coherently, among strategies S1 to S3 the highest pressure increase is registered for S1, which is associated to the highest injected concentration, and decreases with increasing C_{inj}. This observation is consistent with the simulated ripening kinetics for particle attachment, and with experimental results of laboratory injection tests, which indicated an increase in porous medium clogging with increasing concentration of injected suspension (Hosseini and Tosco 2013). However, the simulation results also indicate that, as a general rule, the overall increase in pressure drop is limited when the injection of high concentrations is associated to a short duration, and injection steps are spaced out byflushing steps (strategies S4 to S22): this result is suggested by the lower values of

$C1_{\Delta P}$criterion for the strategies S12-S21 (three injection steps, maximum injected concentration 12.0 *g/l*) compared to strategies S6 to S11 (two injection steps, maximum injected concentration 12.8 *g/l*). Conversely, a higher injection rateheightens the pressure drop during NZVI injection(Figure 5) with negative hydrological effects, but conversely it shortens the flushing time required to remove clogging and to recover the initial conditions.

Criterion $C2_{C/Cinj}$: retained particles

Figure 6shows the results of criterion $C2_{C/Cinj}$, which represents the percentage of injected particles retained within 0.5 *m* from column inlet. The results indicated that strategies S3, S23, S24, and S25 will result in higher mobility of the particles, with lower retained mass. This result also suggests that a lower injection rate increases the mobility ofthe particles. In particular,strategies S23, S24, and S25 correspond to the lowest values of$C2_{C/Cinj}$ (retained mass lower than 3.7%)forthe highest pore water velocity (V= 172.8 m/d), whereas the strategy S1 at the lowest flow rate corresponds to the highest value of $C2_{C/Cinj}$ (93.5%) and therefore to the worst performance.As a general rule, for a given injection strategy, increasing the flow velocity has a significant effect on the mobility of particles, but also the injection strategy has a major impact(see Figure 6).

Examples of breakthrough curves (BTCs) for different injection strategies and flow rates are reported in Figure 7. A multi-modal behavior was observed in the BTC curve during flushing for some strategies, particularly at high flow rates. This behavior corresponds to the concurrence of two different release mechanisms, which were experimentally observed for the nano-Fe/Cu particles. At the early stages offlushing, a first rapid release was registered,while a second, delayed peak was observed during advancedflushing.This result implies that two different

releasemechanisms are occurring in such conditions,namely fast and slow detachment, respectively related to sites 1 and 2 in equations2 and 3. This phenomenonbecomes more relevant whenincreasing the pore water velocity (Figure 7 a).

Figure 8 reports the final profiles of retained particles at the end of the simulation for selected scenarios. It is evident that after the last stress period ($t=t_{exp}$), the particles are mainlyretained in the second part of the domain, since thosein the first part have already been (at least partly) flushed out. In addition, the strategies associated with the longest flushing (10000 *s*) between two subsequent injection periods (strategies S16, S13, S22, S11, S19, S11, S8, and S5) correspond to the most heterogeneous particle distribution along the column (Figure 8a), due to the alternation ofdeposition and release. Also, enhancing the flow velocity (from 43.2 to 86.4 m/d) results in an enhanced NZVI breakthrough at the column outlet(see also Figure 7), and consequently fewer retainedparticles (Figure 8 b) are observed. It is finally worth to mention that, when injecting at higher flow rates, the differences between particle profiles obtained from different strategies are enhanced.

Criterion $C3_{AEP}$: porosity reduction

Figure 9 shows the results of the criterion $C3_{AEP}$ (percentage of reduction in averaged effective porosity AEP) for all strategies with different pore water velocities. The fourth set of strategies (S23 to S25) correspondsthe minimum AEP reduction (0.22% for S23 when V=43.2 m/d), while the first strategy (S1) has the maximum value of $C3_{AEP}$(1.70% when V=172.8 m/d). Lower injection rates and flushing periodsbetween the injections limitthe decrease in AEP. The variation of the AEP as a function of time for strategies S1 (for V=43.2 and 172.8m/d) and S25(for V=43.2 m/d) is reported in Figure 10.

Criterion $C4_K$: permeability reduction

The criterion $C4_K$describesthe variation of the average permeability (K) along the domain at the end of experimental time and is strictly related to criterion $C3_{AEP}$, since changes in porosity are, along with variations in the solid-liquid interface area, one of the two components contributing to changes in permeability. The obtained results are given in the bar-plot of Figure 11in semi-logarithmic scale. The maximum and minimum values of $C4_K$ for the three flow velocities are associated, respectively, to strategy S13 (for V=43.2 m/d) and S25 (for$V$=172.8 m/d). This finding suggests again that clogging is more pronounced when higher inlet concentrations are applied, even if the total injected mass is the same. In addition, decreasing the pore water velocity has a considerable effect on the reduction of sand permeability at the end of the experiment.Figure 12 reports examples of the final profiles of K/K_0 as a function of time for selectedinjection strategies.

Criterion $C5_{L99\%}$: travel distance

The final criterion$C5_{L99\%}$ is associated to thedistance over which 99% of the particles are retained through the column. The obtained results are presented in Figure 13 for different flow velocities. The lowest particle mobility is associated with strategy S1 for a flow velocity of 43.2 m/d, and is equal to approximately 2.0m. Assuming this value as the benchmark (l_b), the travel lengths $L_{99\%}$ obtained for the other strategies are reported as normalized travel distances $L_{99\%}$ in Figure 13. For V=43.2 and 86.4 m/d, the strategy S3 is associated tothe maximum travel length (1.2 l_b and 2.3 l_b), but the impact of the strategy on$L_{99\%}$ is limited compared to that of flow rate:

doubling the flow velocityfrom 43.2 to 86.4 m/d results in almost doubling of the travel length. Increasing the flow velocity to V=172.8 m/d, the impact of the injection strategy is more evident. The strategy S23 corresponds to the maximum particle mobility, equal to $L_{99\%}=5.6l_b$. In general, the injection strategies S23-S25, associated to longer injections at lower concentrations, evidence a longer travel length compared to the other scenarios. This observation suggests that the combined effect of high flow rate and low concentration, which corresponds to a lower deposition rates, promotes the mobility of the particles.

Finally, Figure 14 provides a comparison of the effects of flow rate, injected concentration, and number of injection steps on $L_{99\%}$. Figure 14a shows that, the travel length increases significantly with decreasing concentration of injected suspensions (e.g. S1, S2, S3), as discussed above. Conversely, intermediate flushing steps have a minor impact on $L_{99\%}$: as an example, the reader can compare the travel length for S2-S4 (with oneintermediate flushing) andS12 (with two intermediate flushing). Also, Figure 14b indicates that multi-step injection with increasing C_{inj} (S14 and S17) results in shorter travel distances if compared to multi-step injection with decreasing C_{inj} (S23 to S25).

In conclusion, it is worth to mention that the results of criterion $C5_{L99\%}$ for some scenarios may overestimate the travel length of the nanoparticles when up-scaled to natural aquifer conditions,since in a field injection the flow rate is not constant with changing distance from the injection point, according to the radial flow pattern and aquifer heterogeneity. However, injection strategies resulting in longer travel distances in 1D simulations are also likely to be related to longer travel distances in the field, and this criterion applied to simple 1D simulations can provide a first qualitative indication of the expected radius of influence of a NZVI injection in the field.

Remarks and Conclusions

The transport simulations of nano-*Fe/Cu* particles in 1D porous media provided indications on the influence of different injection strategies on the overall mobility of the particles and clogging of the porous medium. In particular, the effects of alternating injection and flushing steps, of constant or variable inject concentration, and of flow rate and injection duration evidenced that all these phenomena are relevant when identifying the best strategy for NZVI delivery. As a general rule, the injection of larger volumes of NZVI dispersion at lower particle concentration has the minimum impact on the hydrological properties of the porous medium, and results in a more pronounced mobility of the particles. In addition, the pore plugging can be minimized if the injection is limited in time, and if it is stopped before the pressure drop begins to dramatically increase. Under such conditions, further prolonging the injection does not result in a significant increase of the NZVI travel distance, but only in a reduction of porosity and permeability, as evidenced also in simulations of microscale iron injection in radial domains (Tosco et al. 2014). On the other hand, the results of this study also indicate that a gradual variation of particle concentration without intermediate flushing can result in limited clogging and enhanced traveling distance.

Despite these conclusions, maximizing travel length and minimizing clogging are not the only aspects to be taken into account for a successful NZVI application at the field scale. As an example, the stoichiometric ratio of Fe^0 content to the contaminant (*Fe/C*) plays a crucial role in the contaminant reduction, and consequentlyin the remediation process. Therefore, alimit to the decrease of the injected NZVI concentration has to be fixed in order to guarantee a complete remediation. Moreover, it is also important to limit the total injected volume of NZVI slurry. The

injection of large volumes of slurry (and eventually of water, if intermediate flushing steps are applied) may result in long injection operations, high costs, and possible problems in handling large volumes of diluted slurries at the site. Furthermore, if the contaminant is present mainly as dissolved phase, injecting large volumes may result in displacing most of the contaminated water around the injection point. In this case, a further extraction step could be necessary few days after NZVI delivery, to "pull back" the contaminant in the NZVI reactive zone (Velimirovic et al. 2014). This process would increasethe time, the cost, and the risks associated to the remediation.Therefore, a trade-off state existsbetweenthe aspects discussed above: the optimal injection strategy is likely not to be the one which can maximize mobility alone, nor minimize clogging, or the injected volume, but a reasonable compromise among a significant radius of influence with a fairly homogeneous distribution of NZVI, limited clogging, limited volume of iron to be injected, and a final NZVI concentrationsufficient to guarantee fast degradation of the contaminants.

The results herein presented are not to be intended as universal from a quantitative point of view, since they are obtained from transport simulations of a specific type of NZVI. However, the conclusions drawn here by comparing the different injection strategies can be extended to other colloidal systems. Moreover, a general approach forthe identification of effective injection strategies in the delivery of nanoscale particles can be proposed. This approach involves the performance of few targeted column tests, aimed at defining the model coefficients in the range of interest of colloid concentration and flow rate via inverse fitting, and then the application of the transport model in direct mode to simulate different injection scenarios. Further modeling for a more quantitative prediction of the expected radius of influence, particle distribution, and porous medium clogging can then be performed on few selected injection scenarios using more

complex colloid transport simulation tools. In this sense, for example, MNMs can be used, which implements the transport equations (1-7) in radial geometry (Tosco et al. 2014).The approach herein described can be adapted to any kind of colloidal dispersion, and in particular to concentrated suspensions that have strong interactions both between particles and porous medium and among particles themselves (straining, ripening, and consequent clogging), like most dispersions of nanoscale and microscale iron-based particles used in groundwater remediation.

References

Bai, R., and Tien, C. (1999). "Particle deposition under unfavorable surface interactions." J Colloid Interf Sci, 218(2), 488-499.

Bradford, S. A., Simunek, J., Bettahar, M., Van Genuchten, M. T., and Yates, S. R. (2003). "Modeling colloid attachment, straining, and exclusion in saturated porous media." Environmental Science & Technology, 37(10), 2242-2250.

Bunn, R. A., Magelky, R. D., Ryan, J. N., and Elimelech, M. (2002). "Mobilization of natural colloids from an iron oxide-coated sand aquifer: Effect of pH and ionic strength." Environmental Science and Technology, 36(3), 314-322.

Cantrell, K. J., Kaplan, D. I., and Gilmore, T. J. (1997). "Injection of colloidal Fe-0 particles in sand with shear-thinning fluids." Journal of Environmental Engineering-Asce, 123(8), 786-791.

Chen, J. Y., Ko, C. H., Bhattacharjee, S., and Elimelech, M. (2001). "Role of spatial distribution of porous medium surface charge heterogeneity in colloid transport." Colloid Surf. A-Physicochem. Eng. Asp., 191(1-2), 3-15.

Comba, S., Dalmazzo, D., Santagata, E., and Sethi, R. (2011). "Rheological characterization of xanthan suspensions of nanoscale iron for injection in porous media." Journal of Hazardous Materials, 185(2–3), 598-605.

Comba, S., and Sethi, R. (2009). "Stabilization of highly concentrated suspensions of iron nanoparticles using shear-thinning gels of xanthan gum." Water Research, 43(15), 3717-3726.

Cook, S. M. (2009). "Assessing the Use and Application of Zero-Valent Iron Nanoparticle Technology for Remediation at Contaminated Sites ", Jackson State University.

Dalla Vecchia, E., Luna, M., and Sethi, R. (2009). "Transport in Porous Media of Highly Concentrated Iron Micro- and Nanoparticles in the Presence of Xanthan Gum." Environmental Science & Technology, 43(23), 8942-8947.

Fiore, S., and Zanetti, M. C. (2009). "Preliminary Tests Concerning Zero-Valent Iron Efficiency in Inorganic Pollutants Remediation." American Journal of Environmental Sciences, 5, 556-561.

Freyria, F. S., Bonelli, B., Sethi, R., Armandi, M., Belluso, E., and Garrone, E. (2011). "Reactions of Acid Orange 7 with Iron Nanoparticles in Aqueous Solutions." The Journal of Physical Chemistry C, 115(49), 24143-24152.

He, F., and Zhao, D. (2005). "Preparation and characterization of a new class of starch-stabilized bimetallic nanoparticles for degradation of chlorinated hydrocarbons in water." Environmental Science and Technology, 39(9), 3314-3320.

Hosseini, S. M., Ataie-Ashtiani, B., and Kholghi, M. (2011). "Bench-scaled nano-Fe 0 permeable reactive barrier for nitrate removal." Ground Water Monit R, 31(4), 82-94.

Hosseini, S. M., and Tosco, T. (2013). "Transport and retention of high concentrated nano-Fe/Cu particles through highly flow-rated packed sand column." Water Res, 47(1), 326-338.

Huang, Y. H., and Zhang, T. C. (2005). "Modeling of nitrate adsorption and reduction in Fe0-packed columns through impulse loading tests." Journal of Environmental Engineering, 131(8), 1194-1202.

Johnson, R. L., Johnson, G. O. B., Nurmi, J. T., and Tratnyek, P. G. (2009). "Natural organic matter enhanced mobility of nano zerovalent iron." Environmental Science and Technology, 43(14), 5455-5460.

Kanel, S. R., Goswami, R. R., Clement, T. P., Barnett, M. O., and Zhao, D. (2008). "Two dimensional transport characteristics of surface stabilized zero-valent iron nanoparticles in porous media." Environmental Science and Technology, 42(3), 896-900.

Kim, H. J., Phenrat, T., Tilton, R. D., and Lowry, G. V. (2012). "Effect of kaolinite, silica fines and pH on transport of polymer-modified zero valent iron nano-particles in heterogeneous porous media." J Colloid Interf Sci, 370(1), 1-10.

Kim, S. C., Harrington, M. S., and Pui, D. Y. H. (2007). "Experimental study of nanoparticles penetration through commercial filter media." Journal of Nanoparticle Research, 9(1), 117-125.

Noubactep, C., Caré, S., and Crane, R. (2012). "Nanoscale metallic iron for environmental remediation: Prospects and limitations." Water, Air, and Soil Pollution, 223(3), 1363-1382.

Nurmi, J. T., Tratnyek, P. G., Sarathy, V., Baer, D. R., Amonette, J. E., Pecher, K., Wang, C., Linehan, J. C., Matson, D. W., Penn, R. L., and Driessen, M. D. (2005). "Characterization and properties of metallic iron nanoparticles: Spectroscopy,

electrochemistry, and kinetics." Environmental Science and Technology, 39(5), 1221-1230.

Nyer, E. K., and Vance, D. B. (2001). "Nano-scale iron for dehalogenation." Ground Water Monit R, 21(2), 41-+.

Phenrat, T., Cihan, A., Kim, H. J., Mital, M., Illangasekare, T., and Lowry, G. V. (2010). "Transport and deposition of polymer-modified Fe 0 nanoparticles in 2-D heterogeneous porous media: Effects of particle concentration, Fe 0 content, and coatings." Environmental Science and Technology, 44(23), 9086-9093.

Phenrat, T., Fagerlund, F., Illangasekare, T., Lowry, G. V., and Tilton, R. D. (2011). "Polymer-modified Fe 0 nanoparticles target entrapped NAPL in two dimensional porous media: Effect of particle concentration, NAPL saturation, and injection strategy." Environmental Science and Technology, 45(14), 6102-6109.

Phenrat, T., Kim, H. J., Fagerlund, F., Illangasekare, T., and Lowry, G. V. (2010). "Empirical correlations to estimate agglomerate size and deposition during injection of a polyelectrolyte-modified Fe 0 nanoparticle at high particle concentration in saturated sand." Journal of Contaminant Hydrology, 118(3-4), 152-164.

Phenrat, T., Kim, H. J., Fagerlund, F., Illangasekare, T., Tilton, R. D., and Lowry, G. V. (2009). "Particle size distribution, concentration, and magnetic attraction affect transport of polymer-modified Fe0 nanoparticles in sand columns." Environmental Science and Technology, 43(13), 5079-5085.

Phenrat, T., Saleh, N., Sirk, K., Tilton, R. D., and Lowry, G. V. (2007). "Aggregation and sedimentation of aqueous nanoscale zerovalent iron dispersions." Environmental Science & Technology, 41(1), 284-290.

Quinn, J., Geiger, C., Clausen, C., Brooks, K., Coon, C., O'Hara, S., Krug, T., Major, D., Yoon, W. S., Gavaskar, A., and Holdsworth, T. (2005). "Field demonstration of DNAPL dehalogenation using emulsified zero-valent iron." Environmental Science and Technology, 39(5), 1309-1318.

Ryan, J. N., Elimelech, M., Baeseman, J. L., and Magelky, R. D. (2000). "Silica-coated titania and zirconia colloids for subsurface transport field experiments." Environmental Science and Technology, 34(10), 2000-2005.

Sakulchaicharoen, N., O'Carroll, D. M., and Herrera, J. E. (2010). "Enhanced stability and dechlorination activity of pre-synthesis stabilized nanoscale FePd particles." Journal of Contaminant Hydrology, 118(3-4), 117-127.

Saleh, N., Kim, H. J., Phenrat, T., Matyjaszewski, K., Tilton, R. D., and Lowry, G. V. (2008). "Ionic strength and composition affect the mobility of surface-modified Fe-0 nanoparticles in water-saturated sand columns." Environmental Science & Technology, 42(9), 3349-3355.

Saleh, N., Kim, H. J., Phenrat, T., Matyjaszewski, K., Tilton, R. D., and Lowry, G. V. (2008). "Ionic strength and composition affect the mobility of surface-modified fe 0< nanoparticles in water-saturated sand columns." Environmental Science and Technology, 42(9), 3349-3355.

Schrick, B., Hydutsky, B. W., Blough, J. L., and Mallouk, T. E. (2004). "Delivery vehicles for zerovalent metal nanoparticles in soil and groundwater." Chemistry of Materials, 16(11), 2187-2193.

Tiraferri, A., Chen, K. L., Sethi, R., and Elimelech, M. (2008). "Reduced aggregation and sedimentation of zero-valent iron nanoparticles in the presence of guar gum." J Colloid Interf Sci, 324(1-2), 71-79.

Tiraferri, A., and Sethi, R. (2009). "Enhanced transport of zerovalent iron nanoparticles in saturated porous media by guar gum." Journal of Nanoparticle Research, 11(3), 635-645.

Tiraferri, A., Tosco, T., and Sethi, R. (2011). "Transport and retention of microparticles in packed sand columns at low and intermediate ionic strengths: Experiments and mathematical modeling." Environmental Earth Sciences, 63(4), 847-859.

Tosco, T., Bosch, J., Meckenstock, R. U., and Sethi, R. (2012). "Transport of ferrihydrite nanoparticles in saturated porous media: Role of ionic strength and flow rate." Environmental Science and Technology, 46(7), 4008-4015.

Tosco, T., Gastone, F., and Sethi, R. (2014). "Guar gum solutions for improved delivery of iron particles in porous media (Part 2): Iron transport tests and modelling in radial geometry." Journal of Contaminant Hydrology, DOI: http://dx.doi.org/10.1016/j.jconhyd.2014.1006.1014.

Tosco, T., Petrangeli Papini, M., Cruz Viggi, C., and Sethi, R. (2014). "Nanoscale iron particles for groundwater remediation: a review." Journal of Cleaner Production, DOI: 10.1016/j.jclepro.2013.1012.1026.

Tosco, T., and Sethi, R. (2009). "MNM1D: a numerical code for colloid transport in porous media: implementation and validation." American Journal of Environmental Sciences, 5(4), 517-525.

Tosco, T., and Sethi, R. (2010). "Transport of non-newtonian suspensions of highly concentrated micro- and nanoscale iron particles in porous media: A modeling approach." Environmental Science and Technology, 44(23), 9062-9068.

Tosco, T., Tiraferri, A., and Sethi, R. (2009). "Ionic Strength Dependent Transport of Microparticles in Saturated Porous Media: Modeling Mobilization and Immobilization Phenomena under Transient Chemical Conditions." Environmental Science & Technology, 43(12), 4425-4431.

Tratnyek, P. G., and Johnson, R. L. (2006). "Nanotechnologies for environmental cleanup." Nano Today, 1(2), 44-48.

Velimirovic, M., Tosco, T., Uyttebroek, M., Luna, M., Gastone, F., De Boer, C., Klaas, N., Sapion, H., Eisenmann, H., Larsson, P.-O., Braun, J., Sethi, R., and Bastiaens, L. (2014). "Field assessment of guar gum stabilized microscale zerovalent iron particles for in-situ remediation of 1,1,1-trichloroethane." Journal of Contaminant Hydrology, 164(0), 88-99.

Westerhoff, P., and James, J. (2003). "Nitrate removal in zero-valent iron packed columns." Water Res, 37(8), 1818-1830.

Xue, D., and Sethi, R. (2012). "Viscoelastic gels of guar and xanthan gum mixtures provide long-term stabilization of iron micro- and nanoparticles." Journal of Nanoparticle Research, 14(11).

Zanetti, M. C., and Fiore, S. (2005). "Evaluation of Mutual Connections between Zero-Valent Iron Reactivity and Groundwater Composition in Trichloroethylene Degradation." Annali di Chimica, 95(11-12), 779-789.

Zhang, W. X. (2003). "Nanoscale iron particles for environmental remediation: An overview." Journal of Nanoparticle Research, 5(3-4), 323-332.

Zolla, V., Freyria, F. S., Sethi, R., and Di Molfetta, A. (2009). "Hydrogeochemical and Biological Processes Affecting the Long-term Performance of an Iron-Based Permeable Reactive Barrier." J. Environ. Qual., 38(3), 897-908.

Figures

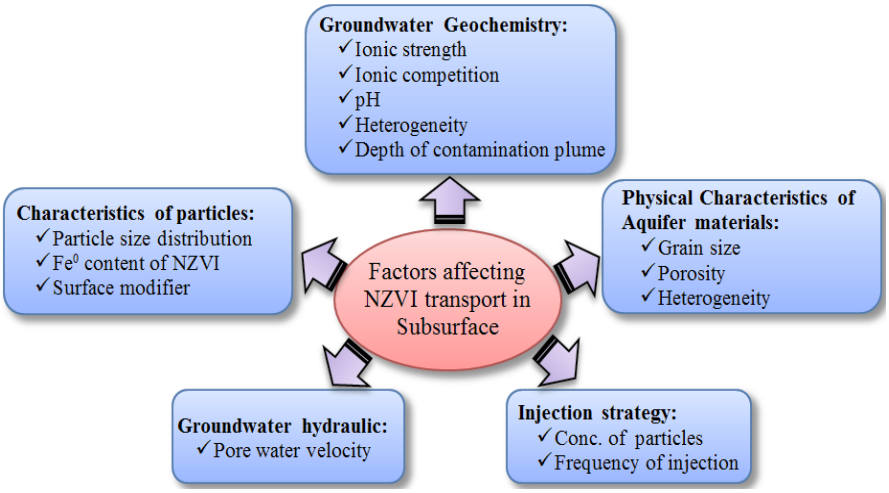

Figure 1: Factors affecting NZVI transport in saturated porous media

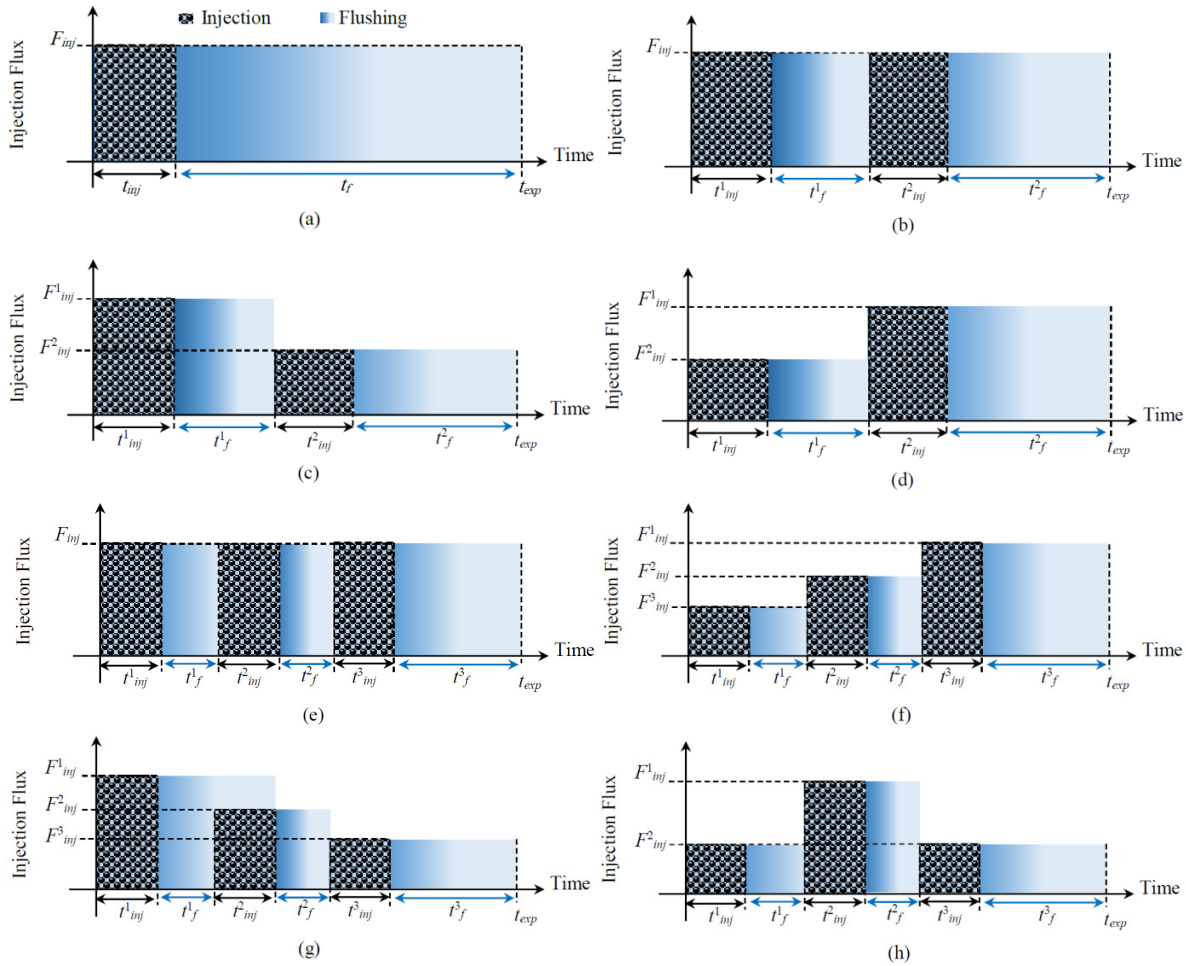

Figure 2: Configuration of the injection strategies for set 1 (a), set 2 (b-d), set 3 (e-h).

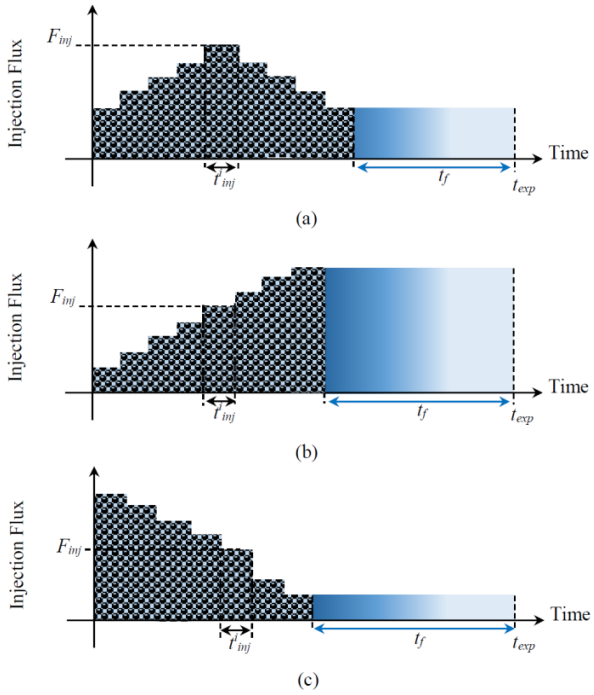

Figure 3: Configuration of the injection strategies of set 4.

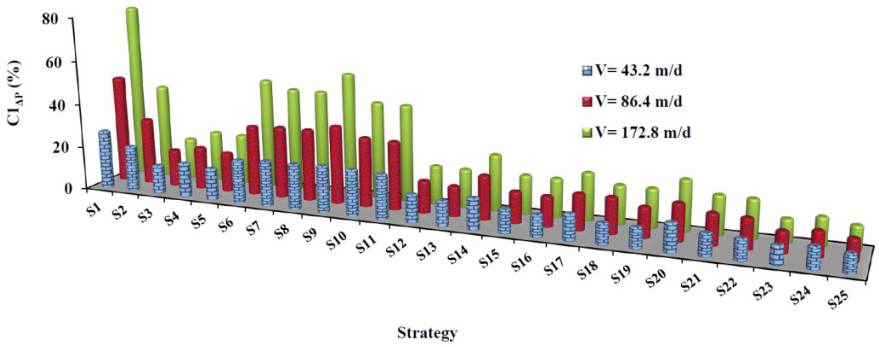

Figure 4: Results of the criterion $C1_{\Delta P}$ for different strategies and pore water velocities.

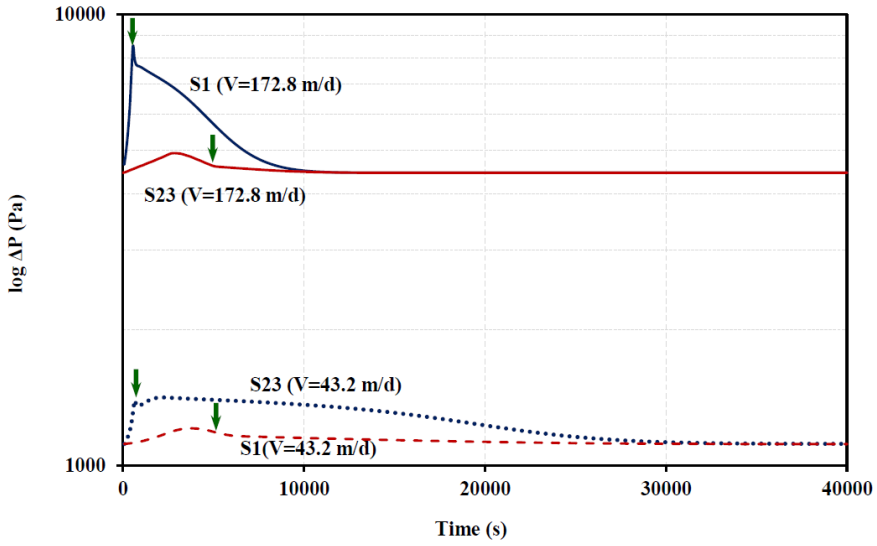

Figure 5: Pressure drop at column ends as a function of time for strategies S1 and S23 with *V*=43.2and *V*=172.8 m/d. The arrows show the end of the NZVI injection in each simulation.

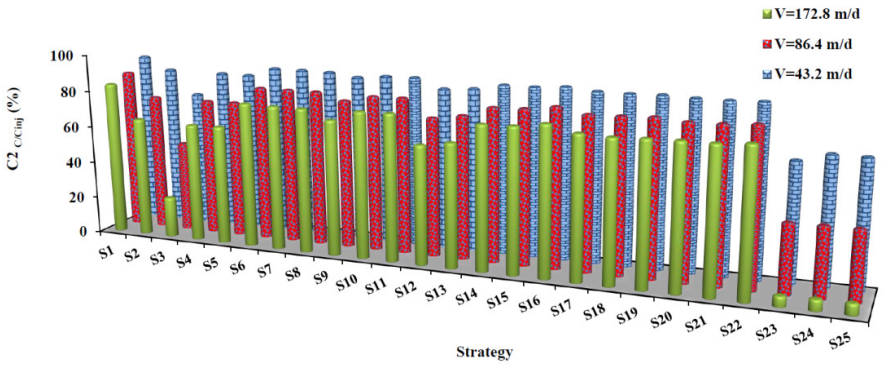

Figure 6: Results of the criterion $C2_{C/Cinj}$ for different strategies and pore water velocities.

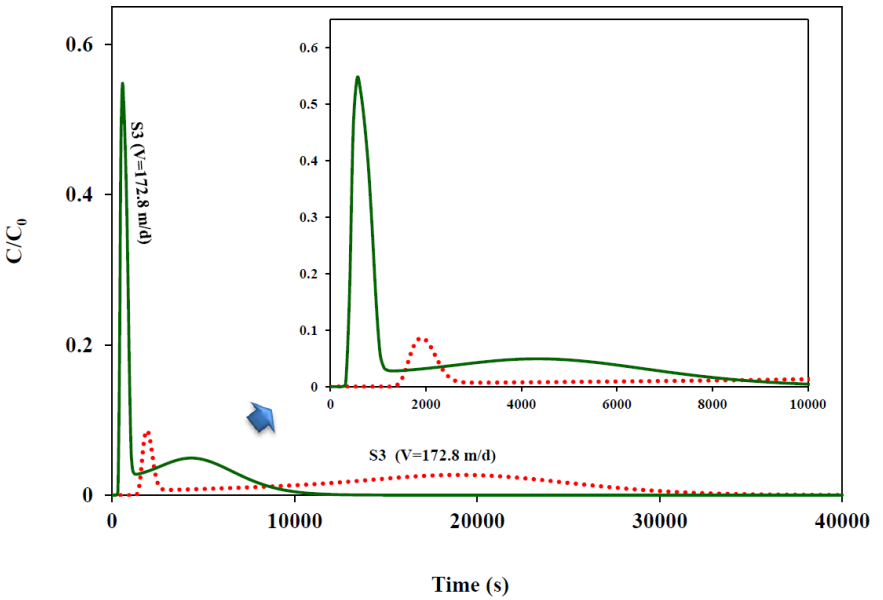

(a)

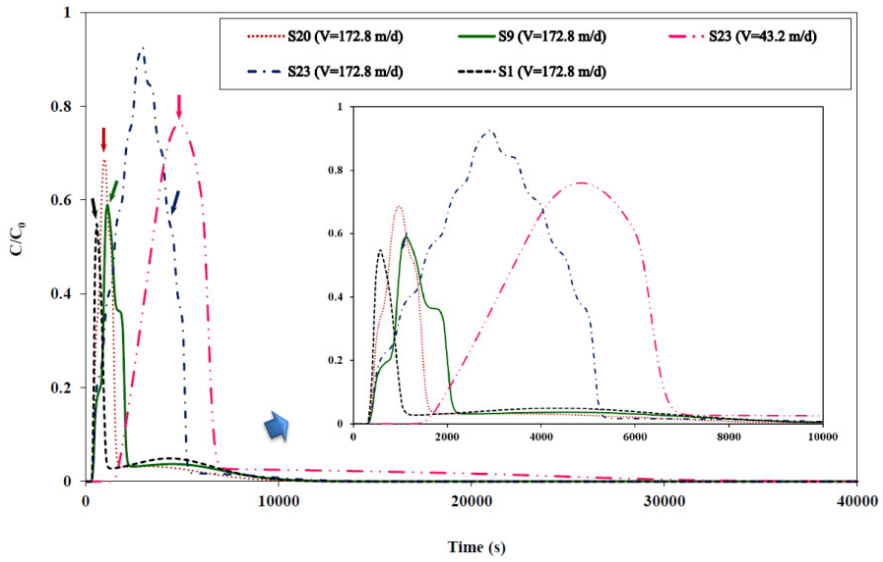

(b)

Figure 7: BTCs at 0.5 *m* for different strategies at different velocities.

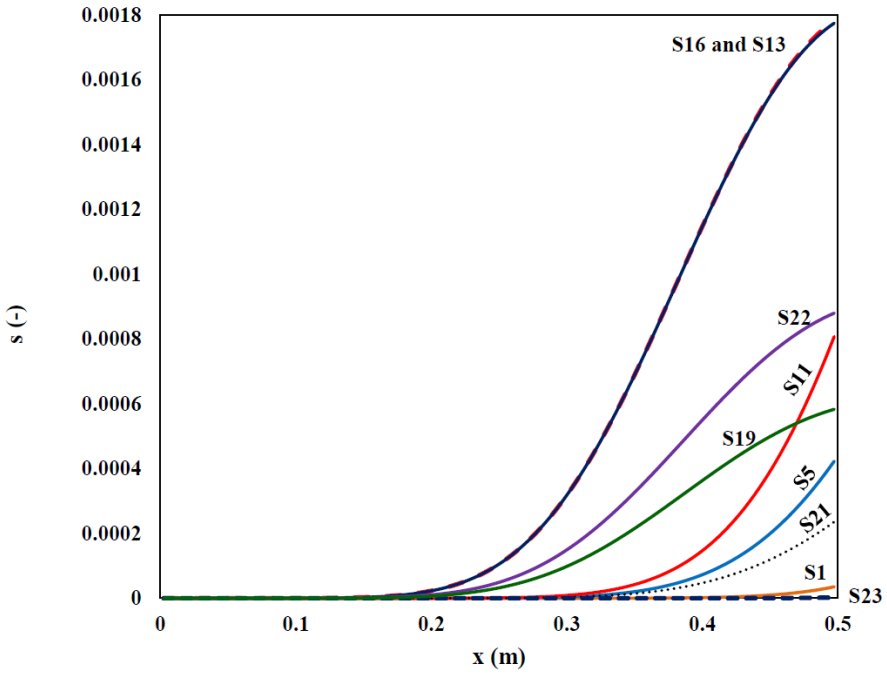

(a)

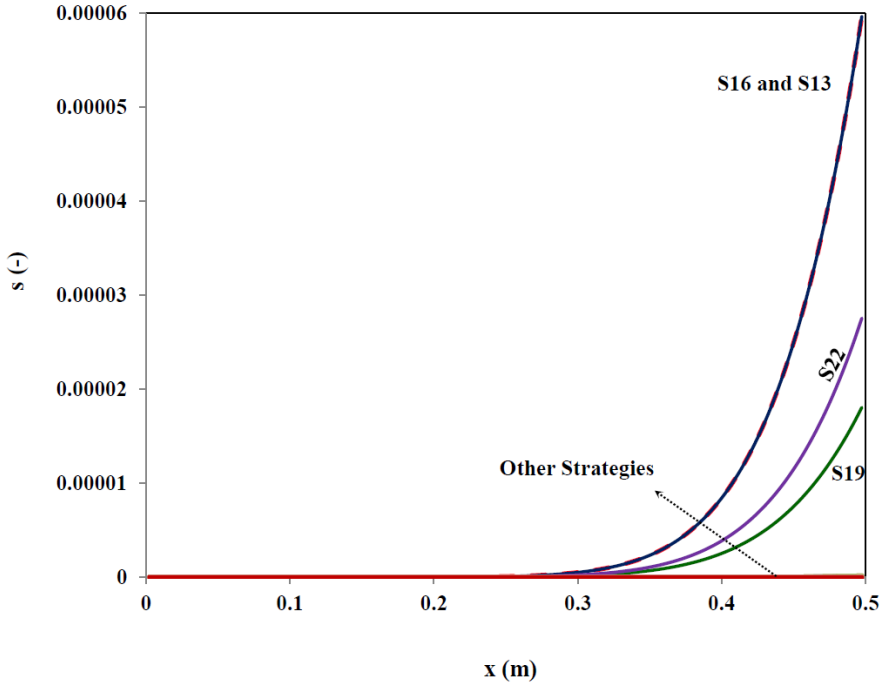

(b)

Figure 8: Examples of final profiles of particle concentration for pore water velocities of a) V=43.2 *m/d*, and b) V= 86.4 *m/d*

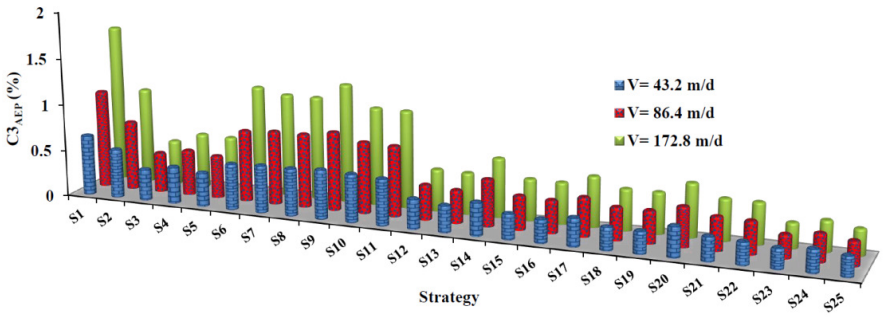

Figure 9: Results of the criterion $C3_{AEP}$ for different strategies and pore water velocities.

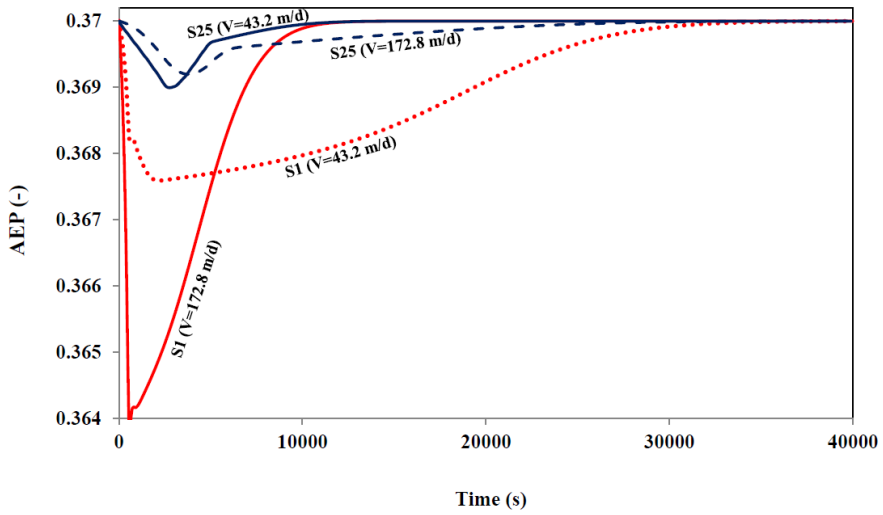

Figure 10: Variation of AEP as a function of time for strategies S1 (V=43.2 and 172.8 m/d) and S25 (V=43.2 and 172.8 m/d).

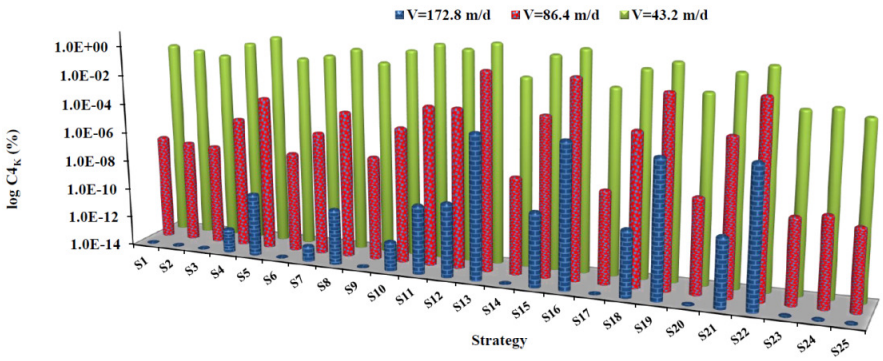

Figure 11:Results of the criterion $C4_K$for different strategies and pore water velocities.

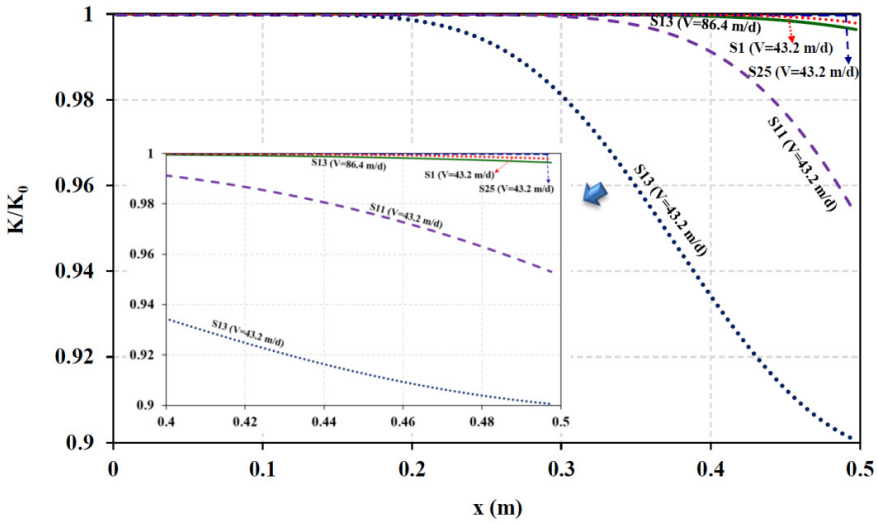

Figure 12: Examples of variation of K/K_0 through the column length for selectedstrategies at the end of the simulation (t_{exp}).

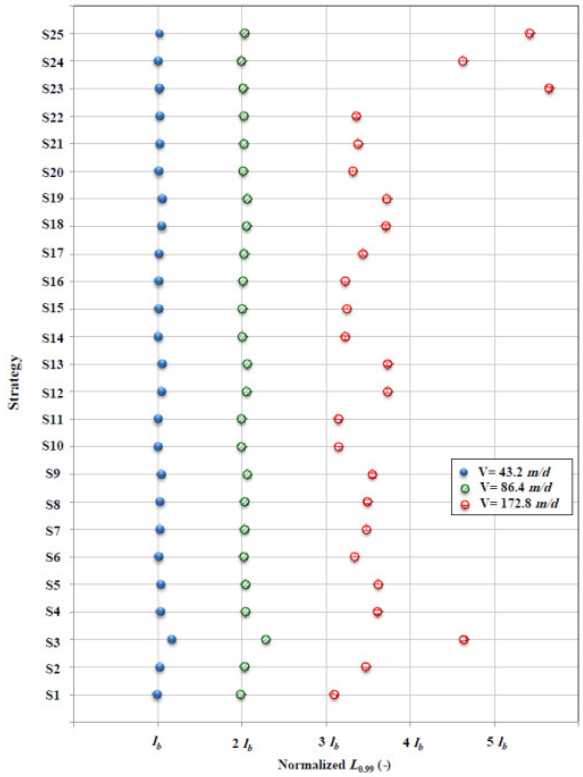

Figure 13: Normalized distance over which 99% of the particles are retained($C5_{L99\%}$)referredto the benchmark value (l_b=2 m) for different strategies and flow rates.

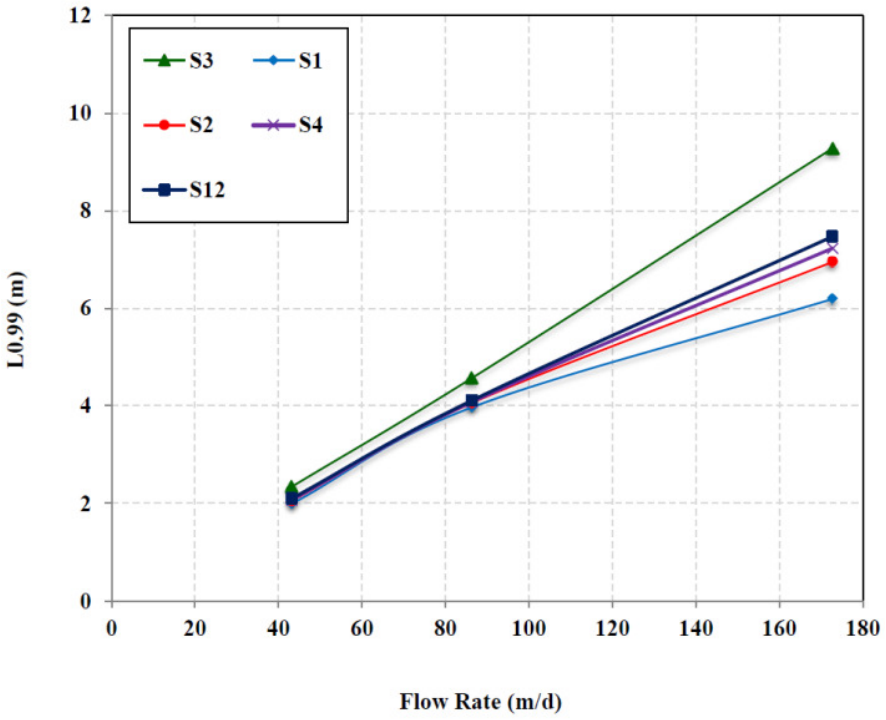

(a)

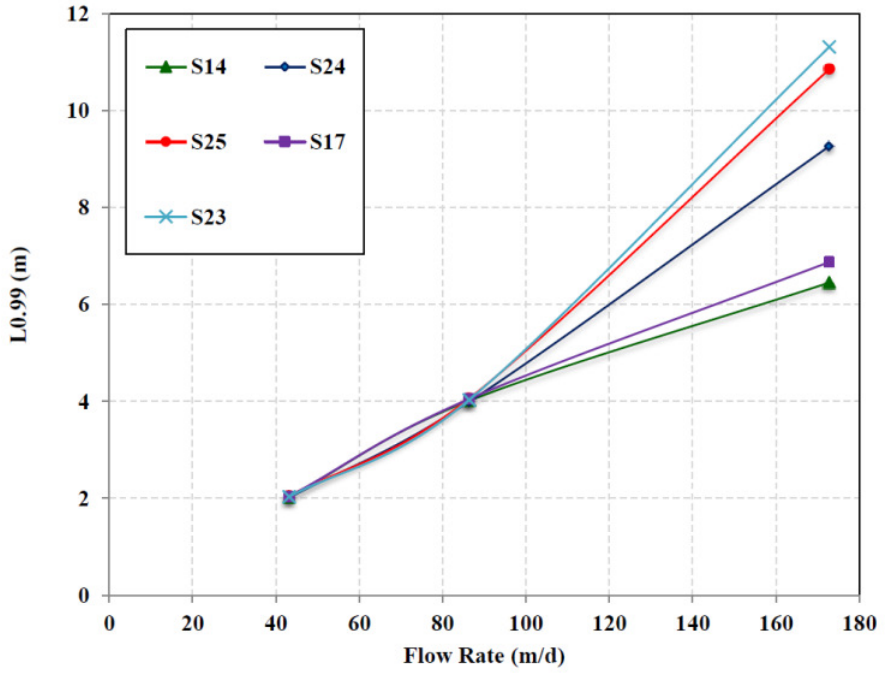

(b)

Figure 14:Comparison of travel lengths $L_{99\%}$for selected injection strategies.

Tables

Table 1: Transport parameters from experimental data fitting (data from Hosseini and Tosco 2013) used in transport simulations with E-MNM1D.

Parameter (unit)	**Parameter Explanation**	**Value**		
		***V*=43.2 m/d**	***V*=86.4 m/d**	***V*=172.8 m/d**
λ (-)	Average degree of packing of the particle deposits	0.371	0.354	0.354
θ (-)	Fraction of deposited nanoparticles contributing to the overall increase of the interface area	0.0036	0.0038	0.0050
k_{a1} (s^{-1})	Deposition rate coefficients for the interaction site 1	0.0060	0.0128	0.0130
k_{d1}(s^{-1})	Release rate coefficients for the interaction site 1	0.016	0.032	0.039
k_{a2}(s^{-1})	Deposition rate coefficients for the interaction site 2	0.042	0.028	0.024
k_{d2}(s^{-1})	Release rate coefficients for the interaction site 2	0.0030	0.0020	0.0032
A_1 (-)	Multiplier coefficients defining the interaction dynamics for site 1	3300	3685	4000
β_1 (-)	Exponent coefficients defining the interaction dynamics for site 1	1.460	1.485	1.510
β_2 (-)	Exponent coefficients defining the interaction dynamics for site 2	0.001	0.012	0.170

Table 2: Typical flow velocity as a function of distance from a pumping well, data from Johnson *et al*. (2009)

Groundwater Velocity ($m\ d^{-1}$)	**Condition**
0.08-0.8	Typical Aquifer
21-52	5m from pumping well
215-520	1m from pumping well
1300-345	Pumping well face

Table 3: Summary of the injection strategies S1 to S22.

#Set	#Strategy	Injected Flux ($gl^{-1}s^{-1}$)			Injected Conc. (gl^{-1})			Stress Periods (s)					
		F^1_{inj}	F^2_{inj}	F^3_{inj}	C^1_{inj}	C^2_{inj}	C^3_{inj}	t^1_{inj}	t^2_{inj}	t^3_{inj}	t^1_{flush}	t^2_{flush}	t^3_{flush}
Set 1	S1	62.10	-	-	16.0	-	-	525	-	-	39475	-	-
	S2	31.05	-	-	8.0	-	-	1050	-	-	37900	-	-
	S3	15.52	-	-	4.0	-	-	2100	-	-	37900	-	-
Set 2	S4	31.05	31.05	-	8.0	8.0	-	525	525	-	5700	33250	-
	S5	31.05	31.05	-	8.0	8.0	-	525	525	-	10000	28950	-
	S6	49.7	12.4	-	12.8	3.2	-	525	525	-	-	38950	-
	S7	49.7	12.4	-	12.8	3.2	-	525	525	-	5700	33250	-
	S8	49.7	12.4	-	12.8	3.2	-	525	525	-	10000	28950	-
	S9	12.4	49.7	-	3.2	12.8	-	525	525	-	-	38950	-
	S10	12.4	49.7	-	3.2	12.8	-	525	525	-	5700	33250	-
	S11	12.4	49.7	-	3.2	12.8	-	525	525	-	10000	28950	-
Set 3	S12	31.05	31.05	31.05	8.0	8.0	8.0	350	350	350	5700	5700	27550
	S13	31.05	31.05	31.05	8.0	8.0	8.0	350	350	350	10000	10000	18950
	S14	10.35	20.70	31.05	3.8	8.2	12.0	350	350	350	-	-	38950
	S15	10.35	20.70	31.05	3.8	8.2	12.0	350	350	350	5700	5700	27550
	S16	10.35	20.70	31.05	3.8	8.2	12.0	350	350	350	10000	10000	18950
	S17	31.05	20.70	10.35	12.0	8.2	3.8	350	350	350	-	-	38950
	S18	31.05	20.70	10.35	12.0	8.2	3.8	350	350	350	5700	5700	27550
	S19	31.05	20.70	10.35	12.0	8.2	3.8	350	350	350	10000	10000	18950
	S20	15.52	31.05	15.52	6.0	12.0	6.0	350	350	350	-	-	38950
	S21	15.52	31.05	15.52	6.0	12.0	6.0	350	350	350	5700	5700	27550
	S22	15.52	31.05	15.52	6.0	12.0	6.0	350	350	350	10000	10000	18950

Table 4: Summary of the injection strategies set 4 (S23 to S25).

# Set	#Strategy	F^i_{inj} $(gl^{-1}s^{-1})$	t^i_{inj} (s)	t_{flush} (s)	C^i_{inj} (gl^{-1})
Set 4	S23	3.35,5.35,7.35,9.35,11.35, 9.35, 7.35,5.35,3.35	525	35275	0.86, 1.38, 1.89, 2.41, 2.92, 2.41, 1.89, 1.38, 0.86
	S24	0.9,2.4,3.9,5.4,6.9,8.4, 9.9,11.4,12.9			0.23, 0.62, 1.0, 1.4, 1.77, 2.16, 2.55, 2.94, 3.3
	S25	12.9,11.4,9.9,8.4,6.9, 5.4,3.9,2.4,0.9			3.3, 2.94, 2.55, 2.16, 1.77, 1.4, 1.0, 0.62, 0.23